Enhancing dynamic origin-destination demand estimation with traffic densities captured from high-resolution satellite imagery

Jiachao Liu[a], Pablo Guarda[b], Koichiro Niinuma[b], Sean Qian[a,c,*]

[a] Department of Civil and Environmental Engineering, Carnegie Mellon University, Pittsburgh, PA, 15213, United States, jiachaol@andrew.cmu.edu

[b] Fujitsu Research of America, Pittsburgh, PA, United States, pguarda@fujitsu.com, kniinuma@fujitsu.com

[c] Heinz College, Carnegie Mellon University, Pittsburgh, PA, 15213, United States, seanqian@cmu.edu

[*] Corresponding author

Extended abstract submitted for presentation at the Conference in Emerging Technologies in Transportation Systems (TRC-30)
September 02-03, 2024, Crete, Greece

April 28, 2024

Keywords: Dynamic network modeling, origin-destination demand estimation, satellite imagery, computational graph

1 INTRODUCTION

The utilization of high-resolution satellite imagery is an increasingly prominent trend in transportation science, offering the potential to enhance existing dynamic network models and address the limitations of traditional data sources (Sakai *et al.*, 2019, Reksten & Salberg, 2021, Ganji *et al.*, 2022). Satellite images provide comprehensive coverage and detailed insights into road networks, traffic patterns, and infrastructure at a scale previously that was previously unachievable with data collected from local sensors. A primary challenge lies in developing a robust calibration framework (i.e., dynamic origin-destination demand estimation, DODE) for large networks that effectively integrates traffic state information (i.e., traffic density) obtained from satellite imagery with other data sources (Ma *et al.*, 2020, Guarda *et al.*, 2024). This study proposes a computational-graph-based DODE framework leveraging multi-source data including traffic densities derived from satellite images and explores the benefits of incorporating satellite imagery into model calibration through numerical experiments using both synthetic and real-world data.

2 FORMULATION

2.1 Formulating multi-class link flow and link density

Following the work of Ma *et al.* (2020), the dynamic assignment ratio (DAR) matrix $\rho^{k,a}_{\text{arr},rs,m}(t_1,t_2)$ serves as the mapping from time-dependent path flow f^{rs}_{m,k,t_1} to link arrival flow $x^{t_2}_{\text{arr},a,m}$. Hence the arrival flow of link a at time t_2 for class m can be modeled as

$$x^{t_2}_{\text{arr},a,m} = \sum_{r,s\in R,S} \sum_{k\in P^{rs}_m} \sum_{t_1\in T_d} \rho^{k,a}_{\text{arr},rs,m}(t_1,t_2)\cdot f^{rs}_{m,k,t_1} \tag{1}$$

f^{rs}_{m,k,t_1} denotes the path flow departing at time t_1 choosing path k between OD pair rs. Shown in Figure 1a, the cumulative arrival flow of link a at timestamp t for vehicle class m, denoted by

$A^t_{a,m}$, can be computed as the summation of all link flow before time t

$$A^t_{a,m} = \sum_{t_2=1}^{t} x^{t_2}_{\text{arr},a,m} \tag{2}$$

where $x^{t_2}_{\text{arr},a,m}$ denotes the arrival flow of vehicle m on link a at time t_2. The DAR matrix $\rho^{k,a}_{\text{arr},rs,m}(t_1,t_2)$ indicates the mapping from time-dependent path flow f^{rs}_{m,k,t_1} to link arrival flow $x^{t_2}_{\text{arr},a,m}$. Similarly, the cumulative departure flow link a at timestamp t for vehicle class m, denoted by $D^t_{a,m}$, can be computed by

$$D^t_{a,m} = \sum_{t_2=1}^{t} x^{t_2}_{\text{dep},a,m} = \sum_{t_2=1}^{t} \sum_{r,s\in R,S} \sum_{k\in P^{rs}_m} \sum_{t_1\in T_d} \rho^{k,a}_{\text{dep},rs,m}(t_1,t_2)\cdot f^{rs}_{m,k,t_1} \tag{3}$$

where $x^{t_2}_{\text{dep},a,m}$ denotes the departure flow of vehicle m on link a at time t_2. The DAR matrix $\rho^{k,a}_{\text{dep},rs,m}(t_1,t_2)$ indicates the mapping from time-dependent path flow f^{rs}_{m,k,t_1} to link departure flow $x^{t_2}_{\text{dep},a,m}$. The difference between cumulative arrival flow and departure flow, divided by segment length, is the density of class m at timestamp t, denoted by $k^t_{a,m}$

$$k^t_{a,m}\cdot l_a = A^t_{a,m} - D^t_{a,m} \tag{4}$$

To obtain more stable and smooth density estimation, we average the densities across several neighboring time intervals around time t, denoted by $[t-\delta, t+\delta]$, the average density can be computed by

$$k^t_{a,m} = \frac{1}{2\delta+1}\sum_{t'=t-\delta}^{t+\delta} k^{t'}_{a,m} \tag{5}$$

Since link lengths (l_a) depend only on link configurations, we use $k^t_{a,m}$ to represent the density which is the vehicle number accumulated on the link at timestamp t. In vectorized form, we use aggregation matrix $\boldsymbol{N}_m$ to perform the summation with respect to time before t.

$$\hat{\boldsymbol{k}} = \sum_{m\in C}(\boldsymbol{A}_m - \boldsymbol{D}_m) = \sum_{m\in C}\left(\boldsymbol{N}_m\boldsymbol{\rho}_m\boldsymbol{p}_m\boldsymbol{q}_m - \boldsymbol{N}_m\boldsymbol{\rho}'_m\boldsymbol{p}_m\boldsymbol{q}_m\right) \tag{6}$$

2.2 DODE formulation

The DODE problem can be formulated as a mathematical programming with travel behavior and network flow dynamic constraints, shown as Equation 7.

$$\begin{aligned}
\min_{\{\boldsymbol{q}_m\}_m} \quad L = {} & w_1 \underbrace{\left(\left\|\boldsymbol{y} - \sum_{m\in C}\boldsymbol{L}_m\boldsymbol{\rho}_m\boldsymbol{p}_m\boldsymbol{q}_m\right\|_2^2\right)}_{L_1} + w_2 \underbrace{\left(\left\|\boldsymbol{z} - \sum_{m\in C}\boldsymbol{M}_m\bar{\Lambda}\left(\boldsymbol{\rho}_m\boldsymbol{p}_m\boldsymbol{q}_m\right)\right\|_2^2\right)}_{L_2} + \\
& w_3 \underbrace{\left(\left\|\boldsymbol{k} - \sum_{m\in C}\left(\boldsymbol{N}_m\boldsymbol{\rho}_m\boldsymbol{p}_m\boldsymbol{q}_m - \boldsymbol{N}_m\boldsymbol{\rho}'_m\boldsymbol{p}_m\boldsymbol{q}_m\right)\right\|_2^2\right)}_{L_3} \\
\text{s.t.} \quad & \{\boldsymbol{h}_m, \boldsymbol{\rho}_m, \boldsymbol{\rho}'_m\}_m = \Lambda(\{\boldsymbol{f}_m\}_m) \\
& \boldsymbol{f}_m = \boldsymbol{p}_m\boldsymbol{q}_m \\
& \boldsymbol{p}_m = \Psi_m(\{\boldsymbol{c}_m\}_m, \{\boldsymbol{h}_m\}_m) \\
& \boldsymbol{q}_m \geq 0, \forall m \in C
\end{aligned} \tag{7}$$

where $\boldsymbol{y}$, $\boldsymbol{z}$ and $\boldsymbol{k}$ are observed count, travel time and density. $\boldsymbol{L}_m$, $\boldsymbol{M}_m$ and $\boldsymbol{N}_m$ are aggregation matrices used to map simulated conditions to observed conditions. The objective function is minimizing the differences between modeled and observed traffic conditions including link traffic count, link travel time and link density. The constraints are behavior model such as route choice function Ψ, and dynamic network loading (DNL) function Λ. The route choice function use path

and link travel cost ($\boldsymbol{c}_m$ and $\boldsymbol{h}_m$) as inputs and outputs route choice proportion $\boldsymbol{p}_m$. The Λ function loads path flow $\boldsymbol{f}_m$ in the network and outputs link travel time $\boldsymbol{h}_m$ and DAR matrices $\boldsymbol{\rho}_m$ and $\boldsymbol{\rho}_m^{'}$. We use the $\bar{\Lambda}$ to indicate the relationship between link arrival flow $\boldsymbol{x}_m = \boldsymbol{\rho}_m \boldsymbol{p}_m \boldsymbol{q}_m$ and link travel time $\boldsymbol{h}_m$, denoted by $\boldsymbol{h}_m = \bar{\Lambda}(\boldsymbol{x}_m)$.

The formulation can be presented on a computational graph (Figure 1b) and solved by forward-backward algorithms efficiently. In the forward pass, a dynamic traffic assignment (DTA) problem is solved using behavior function Ψ and DNL model Λ given fixed demand $\boldsymbol{q}_m$. Route choices and link-level traffic states are obtained. During the DNL, dynamic assignment ratios (DAR) are recorded and the DNL process can be approximated in a linear manner using route choice proportion and DARs. In the backward process, the gradient of loss function with respect to demand is computed, following Equation 8. Any gradient based solution algorithm can be used to solve the DODE on the computational graph.

$$\begin{aligned}\frac{\partial L}{\partial \boldsymbol{q}_m} =& -2w_1 \boldsymbol{p}_m^T \boldsymbol{\rho}_m^T \boldsymbol{L}_m^T \left(\boldsymbol{y} - \sum_{m \in C} \boldsymbol{L}_m \boldsymbol{\rho}_m \boldsymbol{p}_m \boldsymbol{q}_m \right) - 2w_2 \boldsymbol{p}_m^T \frac{\partial \bar{\Lambda}_m(\{\boldsymbol{f}_m\}_m)}{\partial \boldsymbol{f}_m} \boldsymbol{M}_m^T \left(\boldsymbol{z} - \sum_{m \in C} \boldsymbol{M}_m \boldsymbol{h}_m \right) \\ & - 2w_3 \boldsymbol{p}_m^T \cdot \left(\boldsymbol{\rho}_m^T \boldsymbol{N}_m^T - \boldsymbol{\rho}_m^{'T} \boldsymbol{N}_m^T \right) \cdot \left[\boldsymbol{k} - \sum_{m \in C} \left(\boldsymbol{N}_m \boldsymbol{\rho}_m \boldsymbol{p}_m \boldsymbol{q}_m - \boldsymbol{N}_m \boldsymbol{\rho}_m' \boldsymbol{p}_m \boldsymbol{q}_m \right) \right]\end{aligned} \tag{8}$$

3 EXPERIMENTS

The first numerical experiment is conducted on a small network (18 links) with synthetic data. Figures 2 show the comparison of traffic state estimation of Out-of-sample (OOS) links on toy network. As can be seen, the R-squares are all higher in the scenario with density observations, indicating that incorporating density into the calibration can help improve the estimation of unobserved OOS links in terms of all traffic conditions (i.e., link count, travel time and density). We also test our framework on a real-world network around Pittsburgh City, consisting of 16144 links. The densities are captured from a satellite image of Pittsburgh Downtown area. The R-squares for traffic counts travel times of observed links are shown in the Figure 3. It can be seen that adding density observation for large-scale network calibration may decrease the estimation accuracy of observed links. This can be explained by the incompatibility for different data sources. However, examining the estimation results for unobserved OOS links reveals that integrating density with other data can enhance accuracy during some certain periods. For example, the OOS link (ID 2656) is a critical part of the I-376 in Pittsburgh Downtown area. The traffic count of cars for the interval from 12:15 to 12:30 (time period covering the timestamp of the satellite image used) is estimated to be 228 using observed count and travel time. With density data included, the estimation rises to 626, aligning more closely with the actual observed count of 609.

References

Ganji, Arman, Zhang, Mingqian, & Hatzopoulou, Marianne. 2022. Traffic volume prediction using aerial imagery and sparse data from road counts. *Transportation Research Part C: Emerging Technologies*, **141**(Aug.), 103739.

Guarda, Pablo, Battifarano, Matthew, & Qian, Sean. 2024. Estimating network flow and travel behavior using day-to-day system-level data: A computational graph approach. *Transportation Research Part C: Emerging Technologies*, **158**(Jan.), 104409.

Ma, Wei, Pi, Xidong, & Qian, Sean. 2020. Estimating multi-class dynamic origin-destination demand through a forward-backward algorithm on computational graphs. *Transportation Research Part C: Emerging Technologies*, **119**(August), 102747. arXiv: 1903.04681 Publisher: Elsevier Ltd.

Reksten, Jarle Hamar, & Salberg, Arnt-Børre. 2021. Estimating Traffic in Urban Areas from Very-High Resolution Aerial Images. *International Journal of Remote Sensing*, **42**(3), 865–883.

Sakai, Kengo, Seo, Toru, & Fuse, Takashi. 2019. Traffic density estimation method from small satellite imagery: Towards frequent remote sensing of car traffic. *Pages 1776–1781 of: 2019 IEEE Intelligent Transportation Systems Conference (ITSC)*. Auckland, New Zealand: IEEE.

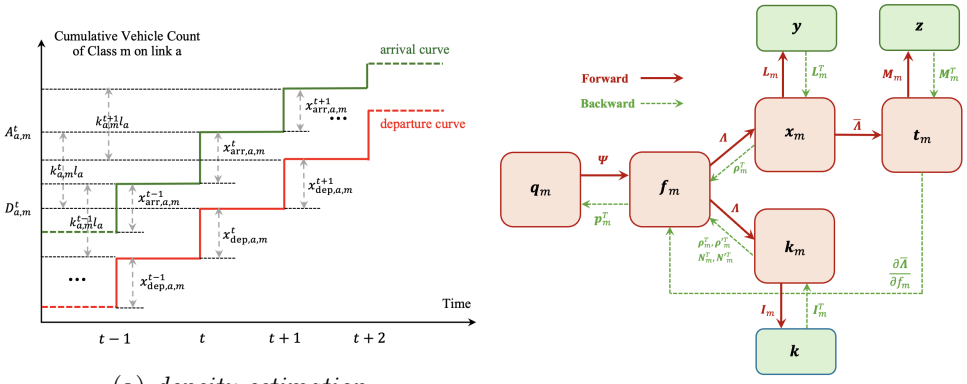

(a) *density estimation* (b) *computational graph*

Figure 1 – *Figures for modeling approach*

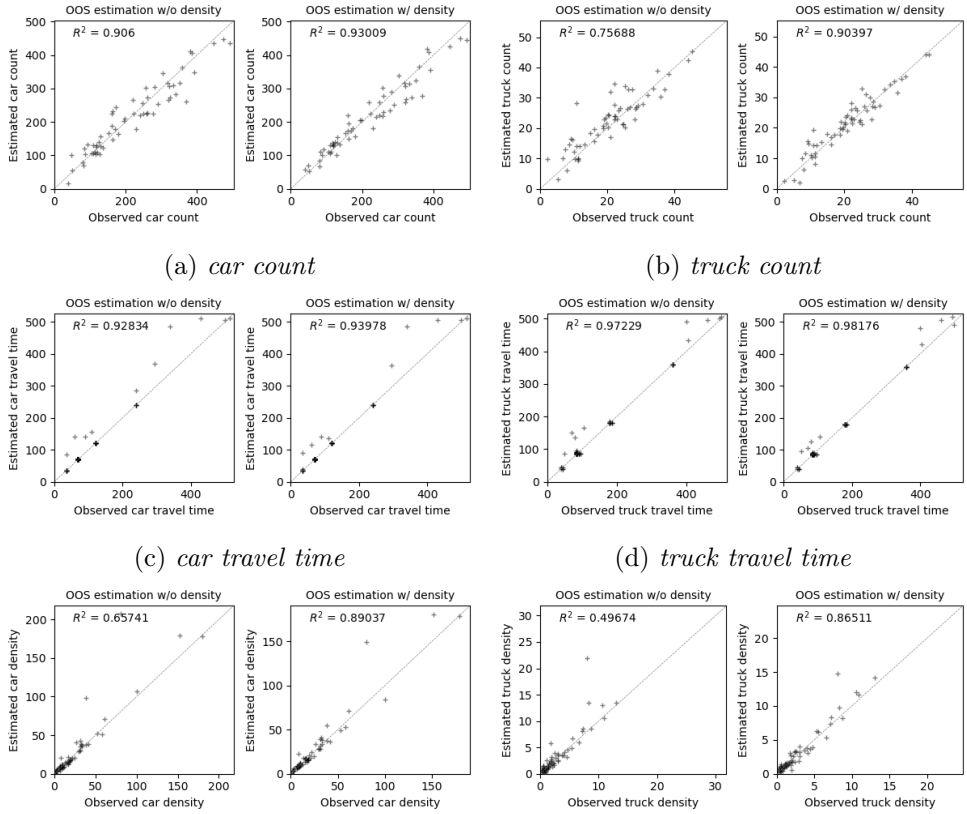

(a) *car count* (b) *truck count*

(c) *car travel time* (d) *truck travel time*

(e) *car density* (f) *truck density*

Figure 2 – *Comparison of traffic state estimation for out-of-samples*

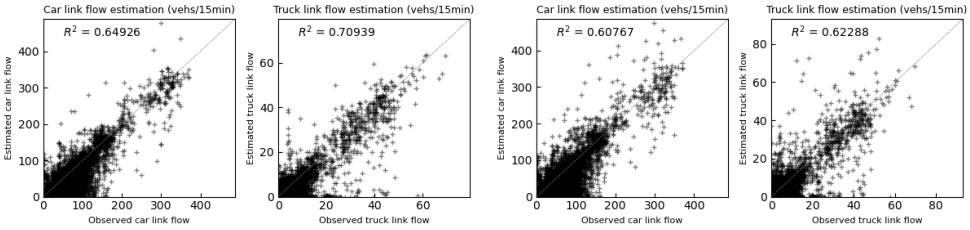

(a) *scenario 1 without density* (b) *scenario 2 with density*

Figure 3 – *Estimation of observed links in two scenarios*